separations

MDPI

Article

New Concept for the Study of the Fluid Dynamics of Lithium Extraction Using Calix[4]arene Derivatives in T-Type Microreactor Systems

Yehezkiel Steven Kurniawan [1,*], Ramachandra Rao Sathuluri [1,2,†], Keisuke Ohto [1], Wataru Iwasaki [2], Hidetaka Kawakita [1], Shintaro Morisada [1], Masaya Miyazaki [3] and Jumina Jumina [4]

1 Department of Chemistry and Applied Chemistry, Faculty of Science and Engineering, Saga University, 1-Honjo, Saga 840-8502, Japan; srrao@nihfw.org (R.R.S.); ohtok@cc.saga-u.ac.jp (K.O.); kawakita@cc.saga-u.ac.jp (H.K.); morisada@cc.saga-u.ac.jp (S.M.)
2 Sensing System Research Center, National Institute of Advanced Industrial Science and Technology, 807-1 Shuku, Tosu, Saga 841-0052, Japan; wataru.iwasaki@aist.go.jp
3 HaKaL Inc., The Juhachi-Shinwa Bank Fukuoka Bldg. 5F, 6-27 NishiNakasu, Fukuoka 810-0002, Japan; miyazaki@hakal-jp.com
4 Department of Chemistry, Faculty of Mathematics and Natural Sciences, Universitas Gadjah Mada, Yogyakarta 55281, Indonesia; jumina@ugm.ac.id
* Correspondence: kurniawan94steven@gmail.com; Tel.: +62-889-9641-4131
† Present address: Department of Reproductive Biomedicine, The National Institute of Health and Family Welfare, Baba Gangnath Marg, Munirka, New Delhi 110067, India.

Citation: Kurniawan, Y.S.; Sathuluri, R.R.; Ohto, K.; Iwasaki, W.; Kawakita, H.; Morisada, S.; Miyazaki, M.; Jumina, J. New Concept for the Study of the Fluid Dynamics of Lithium Extraction Using Calix[4]arene Derivatives in T-Type Microreactor Systems. *Separations* **2021**, *8*, 70. https://doi.org/10.3390/separations8050070

Academic Editor: Marcello Locatelli

Received: 21 April 2021
Accepted: 17 May 2021
Published: 20 May 2021

Abstract: Lithium extraction remains a challenge in the hydrometallurgy process due to its economic value and maldistribution sources. Employing calix[4]arene derivatives in solvent extraction techniques results in high selectivity and extraction capability, but a slow extraction rate. The slow kinetics of batch-wise extraction can be drastically accelerated by using a T-type microreactor system. Therefore, a combination of calix[4]arene and a microreactor system serves as an ideal platform for efficient lithium extraction. In this work, the fluid dynamics of lithium extraction using a monoacetic acid calix[4]arene derivative in a T-type microreactor system were studied. Increasing the O/A ratio increases the average length, surface area, and volume of the organic droplets, but decreases the specific surface area. In contrast, increasing the Reynolds number decreases the average length, surface area, and volume of the organic droplets, but increases the specific surface area. It was found that shorter diffusion distance, larger specific surface area, and faster vortex velocity were the factors that play the most pivotal roles in achieving great extraction rate enhancement in T-type microreactor systems compared to batch-wise systems. These findings represent an important new concept in the study of the fluid dynamics of lithium extraction using monoacetic acid calix[4]arene derivatives in T-type microreactor systems.

Keywords: fluid dynamic; lithium; extraction; calix[4]arene; T-type microreactor; extraction rate; Reynolds number

1. Introduction

Metal elements are pivotal components in electronics, catalysts, and advanced materials that are used in day-to-day life [1]. Lithium is the lightest metal element, and possesses excellent suitability for energy storage applications [2]. Recently, the demand for lithium-ion batteries has increased exponentially due to its irreplaceable role as a carbon-free power energy source in gadgets and appliances [3]. In contrast, the source of lithium is unevenly distributed across the globe thus the recovery of lithium from secondary resources should be considered [4]. Efforts towards lithium recovery have been the focus of researchers around the world for some time, but the recovery process is not easy, because secondary resources are usually composed of various metals that possess similar physicochemical

properties [5,6]. Therefore, the designing a selective and efficient recovery processes is crucial for obtaining promising supplies of lithium in the near future.

The separation of lithium ions (Li(I)) by means of solvent extraction, adsorption, ion-exchange, and membrane filtration has been reported and evaluated [4]. Among these separation techniques, solvent extraction exhibits the simplest method and the highest selectivity for Li(I) extraction [7]. Solvent extraction, also known as liquid–liquid extraction, is a separation technique based on the distribution factor of chemical species in two immiscible solvents. The efficiency of the solvent extraction process strongly depends on the extraction reagent, solvent selection, pH, and other operation conditions [8].

Calixarene is a supramolecular host compound that exhibits remarkable ion discrimination ability in the solvent extraction process [9]. Calixarene has several advantages, such as large-scale synthesis, rigid conformation and structure, and thermal stability [10]. Furthermore, calixarene can be modified at either the upper or lower rim to give it additional functional groups for metal complexation [11–13]. Because of this, calixarene derivatives have been widely applied for metal complexation and metal recovery in recent years [14–16].

Professor Ohto's research group at Saga University, Japan has been focusing on the application of calix[4]arene derivatives for Li(I) extraction [8]. A *tert*-octyl group ($(H_3C)_3C$-CH_2-$C(CH_2)_2$-) was introduced at the upper rim of calix[4]arene to increase the solubility of calix[4]arene in non-polar solvent. Meanwhile, the lower rim of calix[4]arene was modified with ethyl bromoacetate to yield an acetic acid functional group for ion-exchange interaction with Li(I). A series of tetraacetic acid-, triacetic acid-, diacetic acid-, and monoacetic acid-calix[4]arene was synthesized [17], and found that monoacetic acid-calix[4]arene exhibited the highest Li(I) selectivity compared to other alkali and alkaline earth metal ions. The main drawback of solvent extraction using calix[4]arene derivatives is the time-consuming process required as a result of the mass transfer of metal ions being limited by the narrow contact area and thick boundary phase. Table 1 summarizes the extraction of Li(I), sodium (Na(I)), silver (Ag(I)), palladium (Pd(II)), and platinum (Pt(IV)) ions took 1–3 days to reach the equilibrium state [7,18].

Microreactors offer a great enhancement in extraction rate in metal ion extraction processes [19–21]. Therefore, a lot of attention has been devoted to the use of microreactor systems to achieve rapid and efficient chemical processes [22–26]. In previous studies, a T-type microreactor system was employed for metal ions extraction using calix[4]arene derivatives. Ag(I), Pd(II), Pt(IV), Li(I), and Na(I) extractions were performed using MKTOC, ^{2}QuTOC, ^{2}PyTOC, 1Ac, and 3Ac extraction reagents, respectively [7,18]. The chemical structures of these calix[4]arene derivatives are shown in Figure 1. By using a T-type microreactor, the extraction kinetics were accelerated from an order of days to an order of seconds, with a kinetic enhancement factor of 4.3×10^4–1.3×10^5, which is remarkable. However, to the best of the authors' knowledge, the study of the fluid dynamics of metal ion extraction using calix[4]arene derivatives has not been reported, although the fluid dynamics data of metal ion extraction using calix[4]arene derivatives in microreactor systems are critical for understanding why such a great enhancement of extraction rate occurs.

Table 1. Comparison of batch and microreactor system for metal ion extraction.

Metal Ion	Host Compound [a]	Time to Reach Equilibrium in a Batch System	Extraction Rate Enhancement Factor [b]	Reference
Li(I)	1Ac	1 d	4.3×10^4	Kurniawan et al. (2019) [7]
Na(I)	3Ac	1 d	4.3×10^4	Kurniawan et al. (2019) [7]
Ag(I)	MKTOC	3 d	1.3×10^5	Sathuluri et al. (2018) [18]
Pd(II)	^{2}QuTOC	1 d	4.3×10^4	Sathuluri et al. (2018) [18]
Pt(IV)	^{2}PyTOC	1 d	4.3×10^4	Sathuluri et al. (2018) [18]

[a] The chemical structures of the host compounds are shown in Figure 1. [b] Calculated from the ratio between time to reach equilibrium in a batch system compared to a microreactor system (2 s for all metal ions).

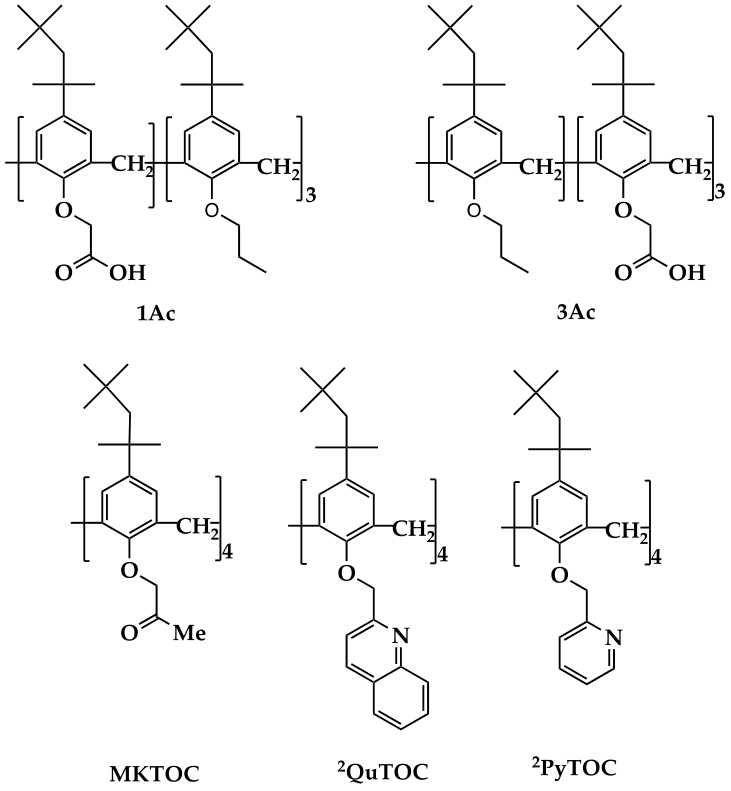

Figure 1. Chemical structures of calix[4]arene derivative as extraction reagent.

In the present work, a study of the fluid dynamics of metal ion extraction using a monoacetic acid calix[4]arene derivative (1Ac) in a T-type microreactor system is reported. Li(I) extraction using 1Ac extraction reagent in chloroform was selected as a representative metal ion extraction process in the microreactor system. At first, the fluid flow pattern between the aqueous and organic phases in the T-type microreactor was investigated. Then, the time required to produce one organic droplet was calculated by varying the organic/aqueous phase (O/A) ratio. The effect of O/A ratio on the length, surface area, volume, and specific surface area of the organic droplet was also studied. Furthermore, the effect of Reynolds number on the length, surface area, volume, and specific surface area of the organic droplet, as well as the vortex velocity inside the organic droplet, was also discussed.

2. Materials and Methods

2.1. Materials

Lithium chloride, ammonia, and chloroform were purchased from Wako Pure Chemicals (Osaka, Japan), while 2-[4-(2-hydroxyethyl)-1-piperazinylethanesulfonic acid] (abbreviated as HEPES), sulfuric acid (98%), and hydrogen peroxide (30%) were purchased from Sigma-Aldrich. The reagents used in this work were of pro-analytical grade and they were employed without any further purification.

2.2. Design of the Microreactor System

The T-type microreactor was fabricated by means of a micro-milling process. The T-shaped microchannel with 200 μm width was drawn using CAD software and the file was transferred to the micro-milling apparatus (MC-ATC-M01; PMT Corp., Fukuoka, Japan). The microchannel, with dimensions of 200 × 200 μm^2, was fabricated from Tempax glass using a diamond-coated needle (0.2 mm diameter). The length of the microchannel was 73 mm. The upper half of the Tempax glass, which serves as a lid for the microchannel, was drilled to form two holes corresponding to the inlets for both the aqueous and the organic phases, and one outlet hole for the collection of both phases after the extraction process.

The 200 × 200 μm^2 dimensions of the microchannel were confirmed by a laser reflection microscope (Keyence VK-8500). Both halves of the microchannel were cleaned with a piranha solution (a mixture of sulfuric acid and hydrogen peroxide in a ratio of 3:1 *v/v*) for 1 h, followed by cleaning three times with distilled water. Afterwards, both halves of the microchannel were permanently bonded through a thermal fusion process. The microreactor device was assembled in a holder (Dolomite), and polytetrafluoroethylene (PTFE) tubes (GL Science Inc., Japan with internal diameter = 0.5 mm) were inserted into both of the inlets and the outlet of the microreactor. The microreactor device was cleaned using 6 mol dm^{-3} KOH followed by rinsing with deionized water prior to use.

2.3. Study of Fluid Dynamics of Li(I) Extraction in a T-Type Microreactor System

The 1Ac derivative was prepared in a similar manner to the procedures described previously [17]. The organic phase was prepared by dissolving the 1Ac extraction reagent in chloroform at a concentration of 5.0 mmol dm^{-3}. Meanwhile, the aqueous phase was prepared by dissolving 0.1 mmol dm^{-3} lithium chloride in 0.1 mol dm^{-3} ammonia and 0.1 mol dm^{-3} HEPES buffer solution at a pH of 9. The density and viscosity of each liquid phase were measured using 10.0 mL pycnometer (TOP®, Tokyo, Japan) and Redwood viscometer (NO W-1410 Kusano Science Corporation, Tokyo, Japan), respectively, at 293 K.

The microreactor system with two high-precision syringe pumps (Model 100, BAS, Tokyo, Japan) to inject the aqueous and organic phases separately from a gastight syringe (GASTIGHT 1001, Hamilton Company, Reno, NV, USA) through a PTFE tube (250.0, 1.6, and 0.5 mm of length, outer, and inner diameters, respectively) into the microchannels. The O/A ratio and Reynolds number were controlled by adjusting the flow rates of the aqueous and organic phases. The optical microscope (Eclipse TS 100, Nikon Corporation, Tokyo, Japan) and a high-speed camera (FASTCAM Mini AX 100, Photoron Limited, Tokyo, Japan with shutter speed 5000 s^{-1}) were used to visualize the organic droplets inside the microchannel. The flow pattern, the time required to form organic droplet, the droplet size, and the vortex velocity were determined on the basis of the photograph images using the Adobe Photoshop software package (Adobe Systems Incorporated, San Jose, CA, USA).

3. Results and Discussion

3.1. Fluid Flow Pattern in a T-Type Microreactor System

In this work, we performed a fluid dynamics study of Li(I) extraction in a T-type microreactor system. The aqueous phase is injected as a continuous phase, while the organic phase is injected as a dispersed phase in the T-type microreactor system resulted in the generation of organic phase droplets in the main microchannel [9]. The T-type microreactor system selected in the present work squeezed strongly the dispersed phase at the T-junction thus extra shear stress enhances the recirculation velocity inside the droplets. Moreover, the shear stress between droplet and the microchannel wall also increases the internal mixing velocity lead diffusion rate and mass transfer enhancement of Li(I) extraction when using 1Ac [27]. It has been reported that 1Ac calix[4]arene derivatives exhibit excellent selectivity for Li(I) ions compared to other alkali and alkaline earth metal ions [17]. Therefore, 1Ac calix[4]arene derivatives in chloroform used as the organic phase and Tempax glass selected as the materials for microchannel fabrication on the basis of its high stability against chloroform [7].

By varying the flow rates of aqueous and organic phases, different fluid phenomena were observed, as shown in Figure 2a. Figure 3 shows the microscopic images of five types of fluid flow pattern, i.e., dripping flow, slug flow, transition region, jetting flow, and parallel flow in the main microchannel. Dripping flow is defined as the organic droplets being in a spherical form while slug flow is defined as the organic droplets being in a capsule-like form [27]. The transition region was defined as an unstable slug flow in which the size of the droplets is not uniform [28]. Meanwhile, jetting flow is defined as a combination of slug flow and parallel flow. This means that fluid flow is parallel until a certain point in the main microchannel and then the droplets are generated [29]. On the

other hand, parallel flow is designated when both aqueous and organic phases flow in the same direction [30].

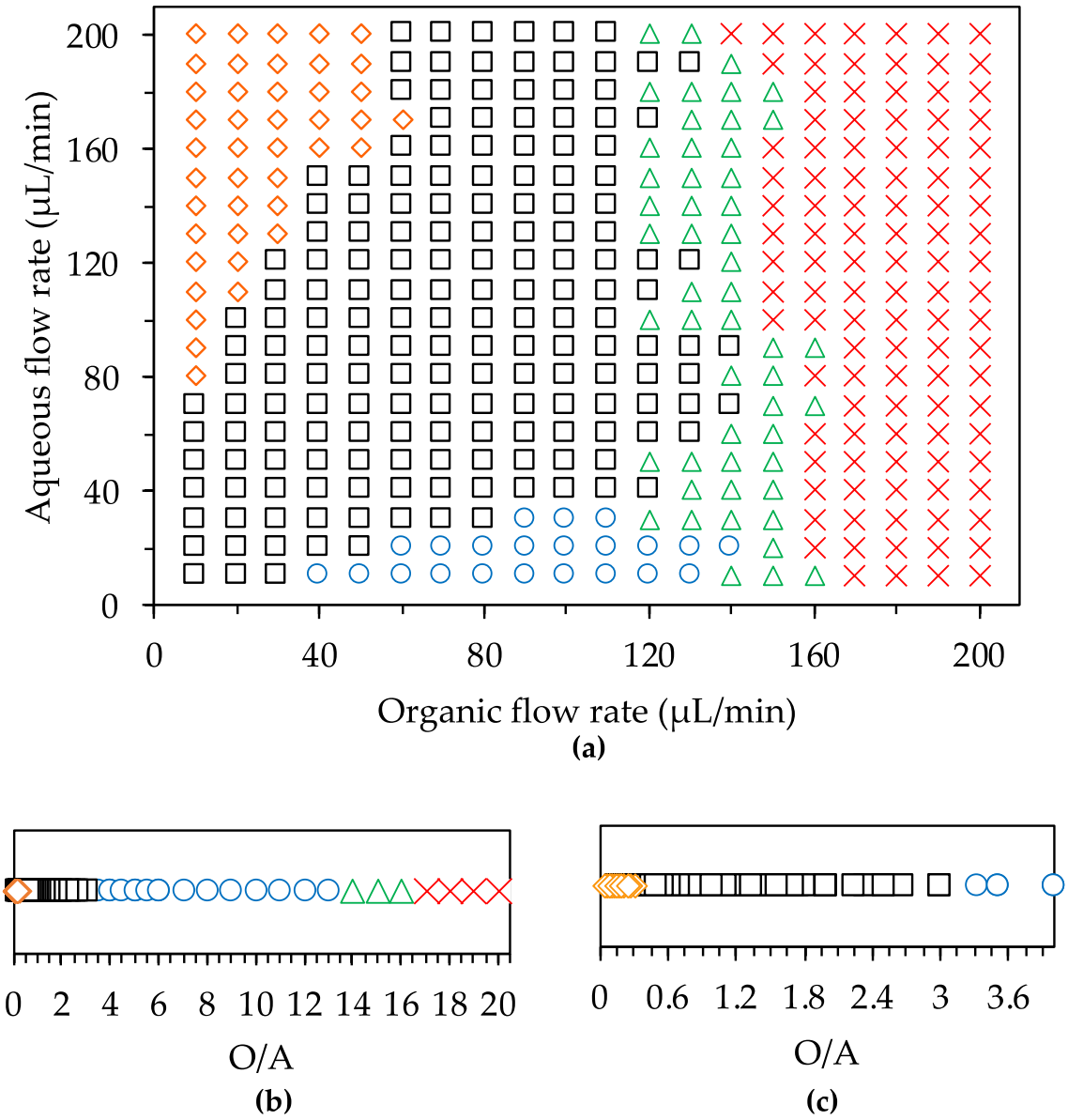

Figure 2. Fluid flow pattern in a T-type microreactor system. (**a**) Flow rate profile when varying the aqueous and organic flow rates. (**b**) Effect of O/A ratio (0–20) on the fluid flow pattern. (**c**) Effect of O/A ratio (0–4.0) on the fluid flow pattern. ◇: dripping flow, □: slug flow, ○: transition region, △: jetting flow, ×: parallel flow.

Interestingly, the fluid flow pattern in the T-type microreactor system is dependent on the organic/aqueous flow rate (O/A) ratio, as shown in Figure 2b. The O/A ratios were calculated by dividing the flow rate of the organic phase by the flow rate of the aqueous phase. When the O/A ratio was less than 0.3, a dripping flow was observed in the microreactor system. The reason for the generation of dripping flow is that the volumetric flow rate of the organic phase is much lower than the volumetric flow rate of the aqueous phase; thus, the organic droplets are observed in a spherical form. Meanwhile, a slug flow pattern was formed when $0.3 < O/A < 3.0$. At higher O/A, a stable slug flow pattern is no longer observed. Jetting and parallel flow patterns occurred when the $13 < O/A < 16$ and $O/A > 16$. Further studies were conducted at $0.3 < O/A < 3.0$ to maintain the stability of the slug flow.

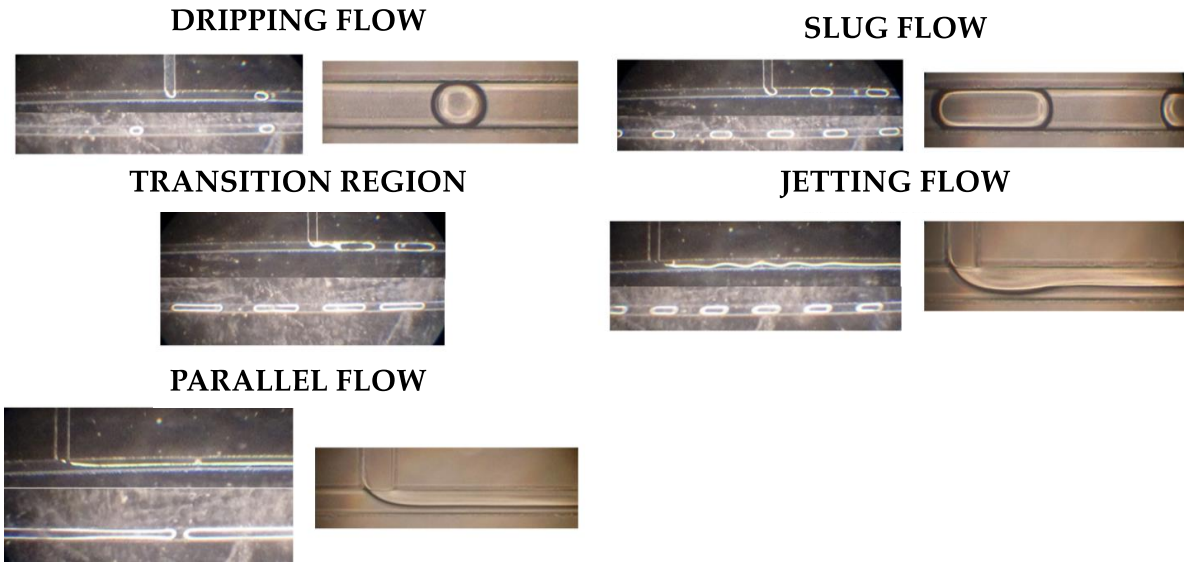

Figure 3. Microscopic images of the fluid flow pattern in a T-type microreactor system.

3.2. Organic Droplet Formation in a T-Type Microreactor System

Figure 4 shows the stepwise mechanism of organic droplet generation at O/A = 1. At first, the organic phase, similar to the dispersed phase, enters the T-junction of the microreactor as a result of the power of the microsyringe pump. Since the microreactor device was fabricated using Tempax glass material, which is hydrophilic in nature, the aqueous phase flows in the space between the organic phase and microchannel wall. When the organic phase was elongated and blocked the microchannel for the aqueous phase entry as the continuous phase, a drop in pressure was generated and squeezed the organic phase to form an organic droplet near the T-junction location [31,32].

3.3. Effect of O/A Ratio on the Fluid Dynamics of Organic Droplets

The effect of O/A ratio on the formation of organic droplets is shown in Figure 5. It can be seen that the organic droplet is generated quickly, on the order of milliseconds (ms). The time required to generate an organic droplet is denoted as t_d. The t_d value for O/A ratios of 0.3, 0.4, 0.5, 0.7, 1.0, 1.5, 2.0, 2.5, and 3.0 was 117.9, 104.8, 92.62, 91.06, 86.60, 90.3, 102.8, 113.6, and 129.2, respectively. The t_d value decreased when increasing the O/A ratio from 0.3 to 1.0 while the t_d value decreased at O/A ratios higher than 1.0. When $0.3 < O/A < 1.0$, the t_d value increased due to a faster flow rate of the organic phase. Meanwhile, the t_d value increased when $1.0 < O/A < 3.0$ due to a slower aqueous flow rate; thus, the "power" to squeeze the organic phase was weaker. An O/A ratio of 1.0 gave the fastest t_d value due to the equal force of both the organic and aqueous phases.

Figure 6 shows the effect of the O/A ratio on the average length, surface area, volume, and specific surface area of organic droplets in a T-type microreactor system. On the basis of Figure 3, it can be seen that increasing O/A ratio from 0.3 to 3.0 gradually changed the fluid flow pattern from dripping flow to slug flow. This means that droplet size increased with a higher O/A ratio. Quantitatively, droplet length was measured on the basis of the photographic images with the help of the Adobe Photoshop software package. The average droplet length is calculated on the basis of twenty photographs of organic droplets. The surface area, volume, and specific surface area of the organic droplets are calculated by assuming an organic droplet in the ideal form of a tube with a half sphere at each end of the tube. The mathematical equations for calculating the surface area (S), volume (V), and specific surface area (a) of the organic droplets are shown in Equations (1)–(3), while d is the diameter of the tube (equal to the width of the microchannel, 200 μm) and L is the droplet length [33].

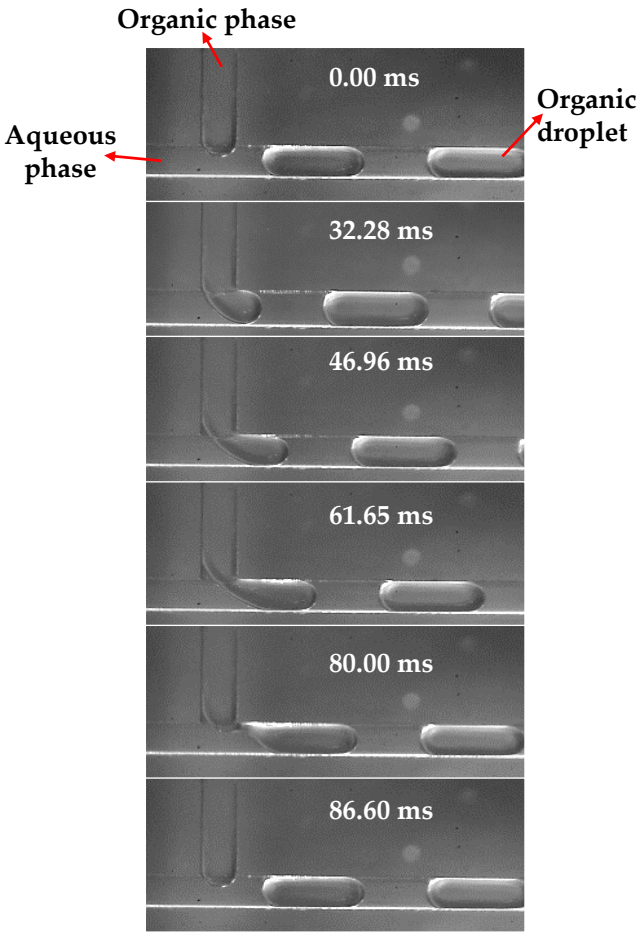

Figure 4. The organic droplet formation in a T-type microreactor system. O/A = 1. Re = 11.58.

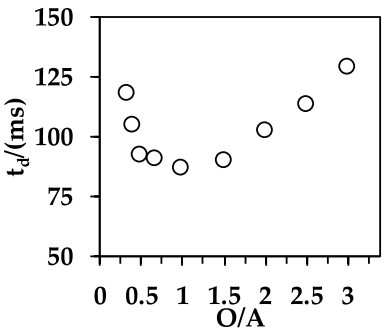

Figure 5. Effect of O/A ratio on the profile of time required to make organic droplet in a T-type microreactor system. Re = 11.58.

$$S = \pi dL \tag{1}$$

$$V = \frac{1}{4}\pi d^2\left(L - \frac{1}{3}d\right) \tag{2}$$

$$a = \frac{S}{V} = \frac{4L}{d\left(L - \frac{1}{3}d\right)} \tag{3}$$

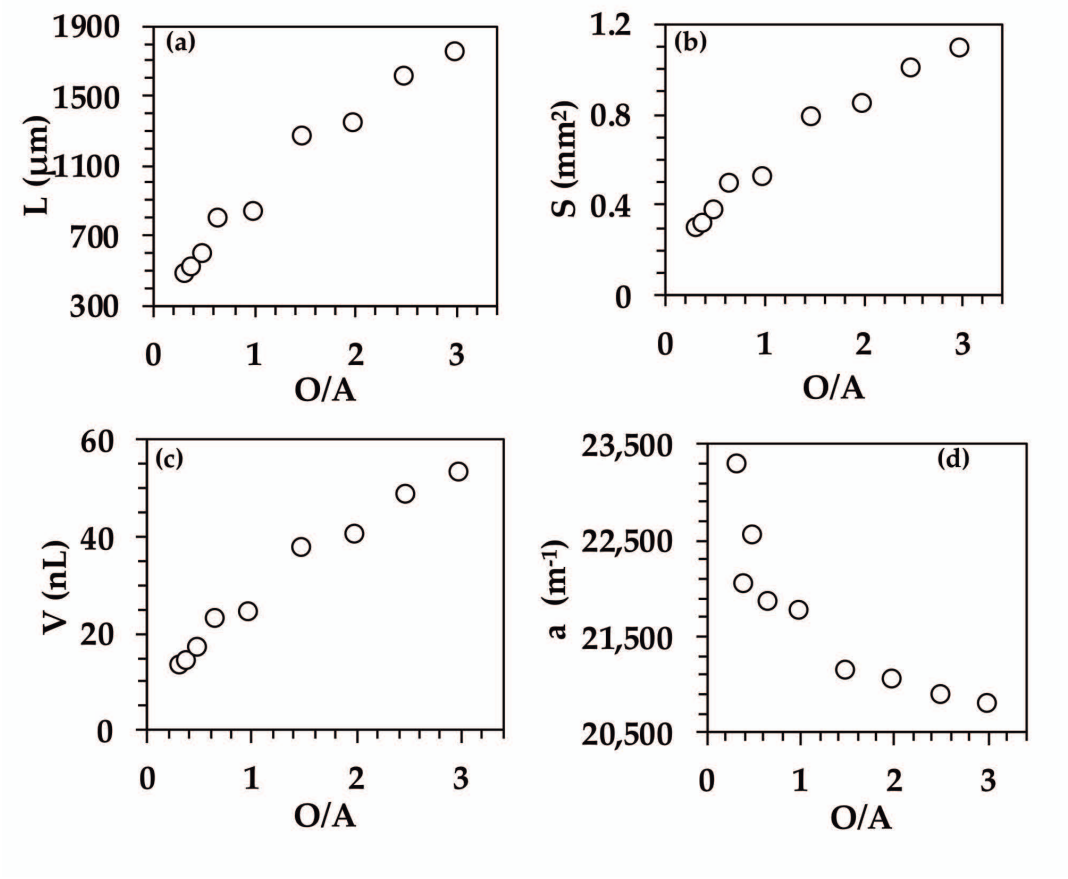

Figure 6. Effect of O/A ratio on the average (**a**) length, (**b**) surface area, (**c**) volume, and (**d**) specific surface area of organic droplets in a T-type microreactor system. Re = 11.58.

On the basis of Figure 6, it can be seen that the average length of the organic droplet increased with increasing O/A ratio. The size of the organic droplet increased from 472.8 to 1742 μm when the O/A ratio was increased from 0.3 to 3.0, respectively. This is because the flow rate of the organic phase is higher when the flow rate of the aqueous phase is lower, thus weakening the squeezing power to cut the organic phase. Since the droplet length was longer, the average surface area and volume of the organic droplets were indeed also larger. Increasing the O/A ratio from 0.3 to 3.0 yielded a droplet surface area in the range of 0.30 to 1.10 mm^2 and a droplet volume in the range of 12.76 to 52.68 nL. In contrast, increasing the O/A ratio from 0.3 to 3.0 decreased the specific surface area of the organic droplets. It is important to note that the calculated average specific surface area of organic droplets was in the range of 20,795–23,283 m^{-1}, which is ~500 times greater than the specific surface area obtained with the commercial batch-wise system (50 m^{-1}). Furthermore, the diffusion distance of the organic droplets (200 μm) was 100 times shorter than that using the batch-wise extraction system (20,000 μm). The large specific surface area and short diffusion distance when using the T-type microreactor system were the reasons for the significant extraction rate enhancement of lithium extraction (see Table 1).

3.4. Effect of Reynolds Number on the Fluid Dynamics of Organic Droplets

The density (ρ) of the aqueous and organic phases was 1012 and 1656 kg m^{-3}, respectively. Meanwhile, the viscosity (μ) of the aqueous and organic phases was 1.086×10^{-3} and 5.219×10^{-4} kg m^{-1} s^{-1}, respectively. Therefore, the Reynolds number was calculated using Equation (4), whereas v is the flow rate of either the organic or the aqueous phase when the O/A ratio is equal to 1.0 [30].

$$\mathrm{Re} = \frac{\rho \, \mathrm{d} \, v}{\mu} = 278.0 \, v \tag{4}$$

Figure 7 shows the effect of Reynolds number on the profile of the time required to make an organic droplet in a T-type microreactor system when the O/A ratio is maintained at 1.0. As reflected in Equation (4), a higher flow rate of either organic or aqueous phase results in a higher Reynolds number. The Reynolds numbers observed in this work are within a range of 3.46–185.3. Outside of this range of Reynolds numbers, the fluid dynamics were not in a stable slug flow pattern (see Figure 2a). It was found that the t_d value decreased when increasing the Reynolds number. The t_d value decreased exponentially from 376.6 to 1.32 ms when increasing the Reynolds number from 3.46 to 185.3. With a higher Reynolds number, shorter t_d values were observed due to the faster flow rate of the organic phase.

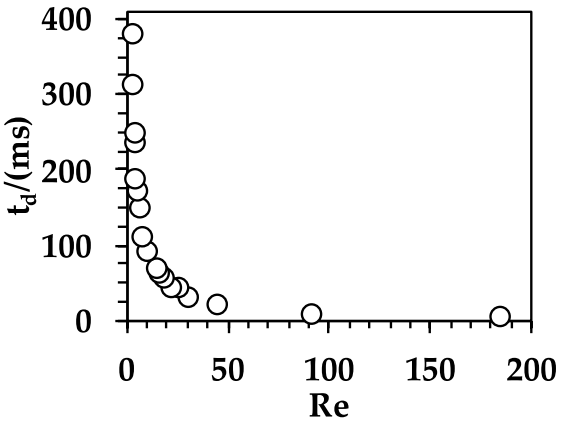

Figure 7. Effect of Reynolds number on the profile of the time required to make an organic droplet in a T-type microreactor system. O/A = 1.0.

Figure 8 shows the effect of Reynolds number on the average length, surface area, volume, and specific surface area of organic droplets in a T-type microreactor system. On the basis of Figure 8, it can be observed that increasing the Reynolds number decreased the droplet size, thus consequently also decreasing the surface area and volume of the organic droplets. The reason for this phenomenon is the faster flow rate of both phases; thus, the t_d value is decreased, and the droplet length is also decreased.

Increasing the Reynolds number resulted in a droplet length in the range of 433.8 to 1152 μm, a droplet surface area in the range of 0.27 to 0.72 mm^2, and a droplet volume in the range of 34.10 to 185.3 nL. On the other hand, increasing the Reynolds number increased the specific surface area of the organic droplets to within a range of 21,229–23,631 m^{-1}. The maximum specific surface area achieved when controlling the Reynolds number (23,631 m^{-1}) was slightly higher than that achieved when controlling the O/A ratio (23,283 m^{-1}). Therefore, further investigations were carried out in order to observe the effect of the Reynolds number on the average vortex velocity (Vr) inside an organic droplet.

It was reported in the previous study that tiny particles were observed during Li(I) extraction using the 1Ac derivative in a microreactor system (see Figure 9a) [7]. The Vr value was calculated by measuring the distance travelled by tiny particles during a certain time on the basis of fifty photographs of organic droplets. Figure 9b shows the effect of the Reynolds number on the Vr value inside organic droplets. It was found that the Vr value was directly proportional to the Reynolds number (R^2 = 0.9948). It is important to note that the length of organic droplets was in the micrometer (μm) dimension, while the Vr value was in the meter (m) dimension (10^6 times higher) in a second. Therefore, the rapid vortex velocity inside organic droplets was another additional reason for the significant enhancement in the extraction rate of Li(I) in the microreactor system. Finally, it was found that short diffusion distance, large surface area, and rapid vortex velocity play pivotal roles in Li(I) extraction in T-type microreactor systems, as shown in Figure 10.

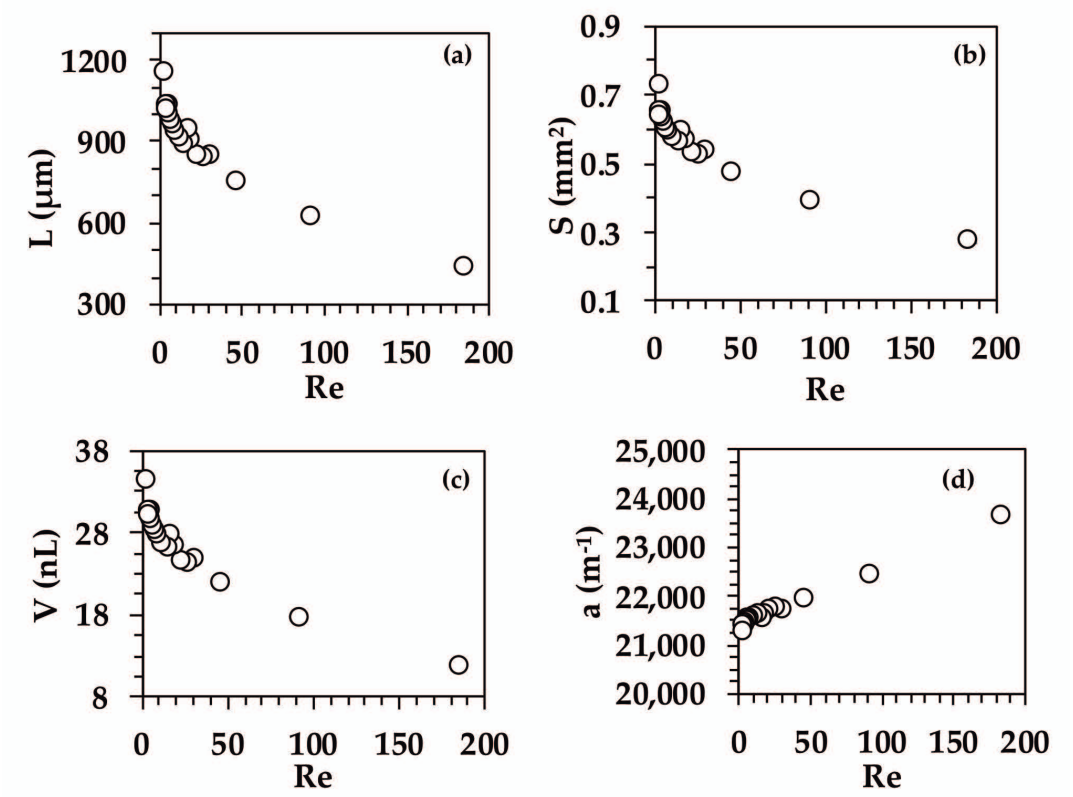

Figure 8. Effect of Reynolds number on the average (**a**) length, (**b**) surface area, (**c**) volume, and (**d**) specific surface area of organic droplets in a T-type microreactor system. O/A = 1.0.

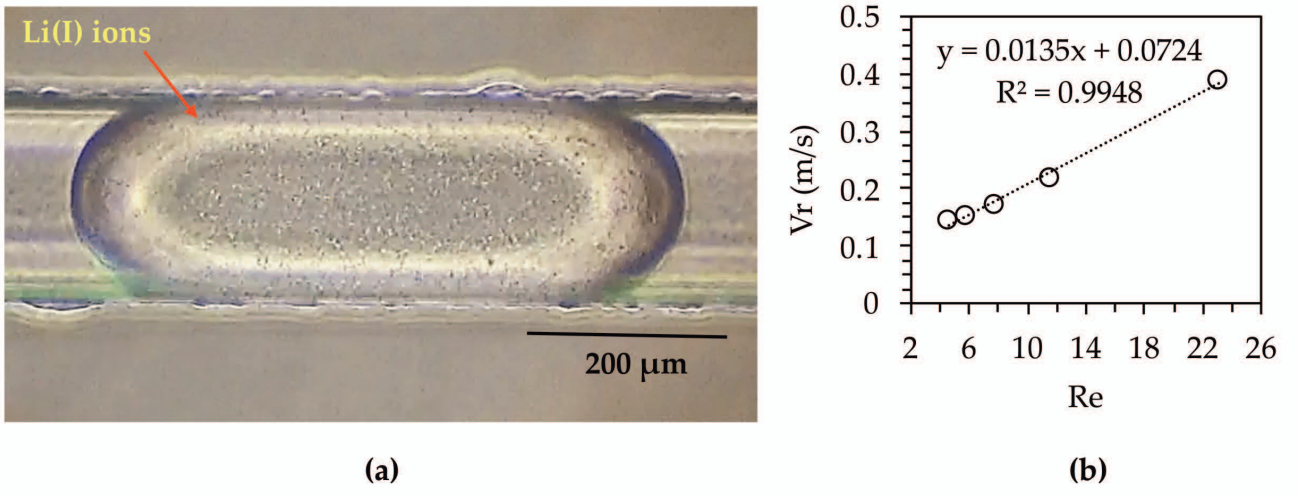

Figure 9. (**a**) Microscopic image of the organic droplets during Li(I) extraction using 1Ac derivative in a T-type microreactor system. (**b**) Effect of Reynolds number on the average vortex velocity inside an organic droplet. O/A = 1.0.

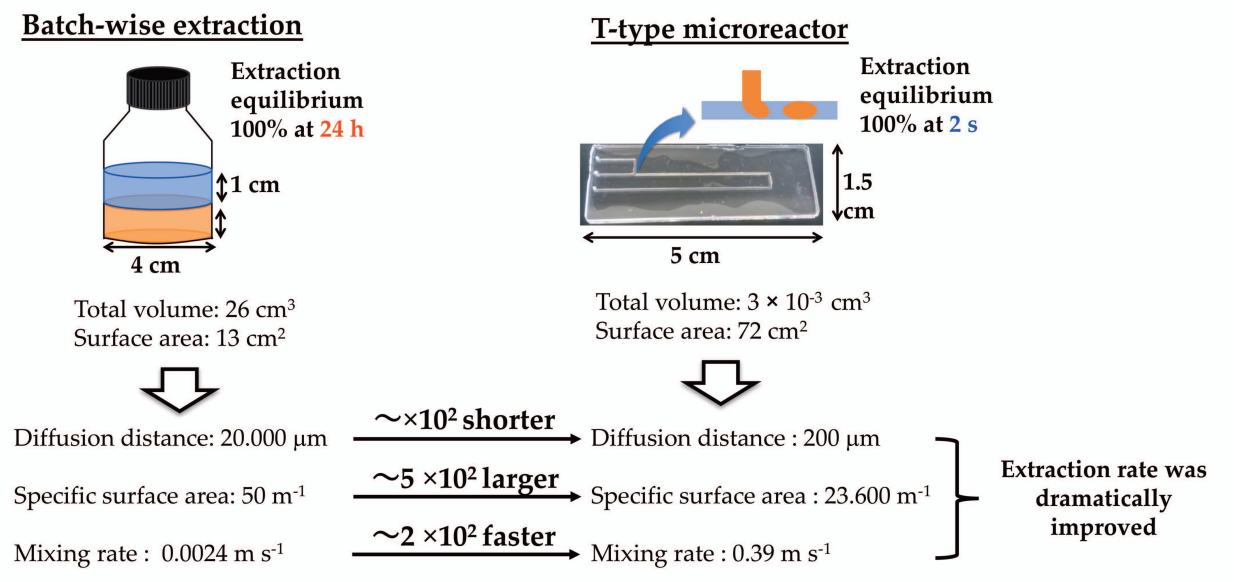

Figure 10. Comparison of the fluid dynamics of Li(I) extraction using 1Ac derivative in the batch-wise and T-type microreactor systems.

4. Conclusions

We carried out a fluid dynamics study of lithium extraction using 1Ac derivative in a T-type microreactor system. The O/A ratio and Reynolds number were controlled by adjusting the flow rates of the aqueous and organic phases using high-precision syringe pumps. The organic droplets inside the microchannel were visualized using an optical microscope with the help of a high-speed camera, and then the images were analyzed to evaluate the flow pattern, the time required to form an organic droplet, the droplet size, and the vortex velocity. Organic phase droplets were generated in the microreactor device, since the aqueous phase was employed as the continuous phase and the T-type microreactor device was fabricated from hydrophilic Tempax glass material. When varying the flow rate of the aqueous and organic phases, five fluid flow patterns were observed, i.e., dripping flow, slug flow, transition region, jetting flow, and parallel flow. A stable slug flow generation was observed at O/A ratios in the range of 0.3–3.0. The shortest time required to form an organic droplet was observed at O/A ratio of 1.0. Increasing the O/A ratio increased the average length, surface area, and volume of the organic droplets, but decreased the specific surface area. In contrast, increasing the Reynolds number decreased the average length, surface area, and volume of the organic droplets, but increased the specific surface area. Compared to batch-wise extraction systems, the lithium extraction rate was drastically enhanced when using the T-type microreactor system, due to shorter diffusion distance, the larger specific surface area, and the faster vortex velocity inside the organic droplets. These results reveal a new concept regarding the fluid dynamics of lithium extraction using calix[4]arene derivatives in T-type microreactor systems.

Author Contributions: K.O. and W.I. conceived and designed the experiments; Y.S.K. performed the experiments; Y.S.K., R.R.S. and H.K. analyzed the data; S.M., W.I., M.M. and J.J. contributed materials/analysis instrument; Y.S.K. and R.R.S. wrote and revised the paper. All authors have read and agreed to the published version of the manuscript.

Funding: The financial support from the collaborative research expenses of the graduate school partnership between Graduate School of Science and Engineering, Saga University and Advanced Industrial Science and Technology Kyushu is greatly acknowledged.

Institutional Review Board Statement: Not applicable.

Informed Consent Statement: Not applicable.

Data Availability Statement: Data are available from the authors upon the reasonable request.

Acknowledgments: The authors would like to acknowledge Kazuma Matsuura, Mizuki Ryu, and Mayumi Fusumada for their technical assistance during the experiment.

Conflicts of Interest: The authors declare that there is no conflict of interest.

References

1. Kaya, M. Recovery of metals and nonmetals from electronic waste by physical and chemical recycling processes. *Waste Manag.* **2016**, *57*, 64–90. [CrossRef] [PubMed]
2. Tarascon, J.M. Is lithium the new gold? *Nat. Chem.* **2010**, *2*, 510. [CrossRef] [PubMed]
3. He, Y.F.; Chu, D.Y.; Zhuo, Z. Cycle stability of dual-phase lithium titanate (LTO)/TiO_2 nanowires as lithium battery anode. *J. Multidiscip. Appl. Nat. Sci.* **2021**, *1*, 54–61. [CrossRef]
4. Swain, B. Recovery and recycling of lithium: A review. *Sep. Purif. Technol.* **2017**, *172*, 388–403. [CrossRef]
5. Muto, A.; Hirayama, Y.; Tokumoto, H.; Matsuoka, A.; Noishiki, K. Liquid-liquid extraction of lithium ions using a slug flow microreactor: Effect of extraction reagent and microtube material. *Solvent Extr. Ion. Exch.* **2016**, *35*, 61–73. [CrossRef]
6. Hirayama, Y.; Hinoue, M.; Tokumoto, H.; Matsuoka, A.; Noishiki, K.; Muto, A. Liquid-liquid extraction and separation of cobalt and lithium ions using a slug flow microreactor. *J. Chem. Eng. Jpn.* **2018**, *51*, 222–228. [CrossRef]
7. Kurniawan, Y.S.; Sathuluri, R.R.; Ohto, K.; Iwasaki, W.; Kawakita, H.; Morisada, S.; Miyazaki, M.; Jumina, J. A rapid and efficient lithium-ion recovery from seawater with tripropyl-monoacetic acid calix[4]arene derivative employing droplet-based microfluidic reactor system. *Sep. Purif. Technol.* **2019**, *211*, 925–934. [CrossRef]
8. Xie, F.; Zhang, T.A.; Dreisinger, D.; Doyle, F. A critical review on solvent extraction of rare earths from aqueous solutions. *Miner. Eng.* **2014**, *56*, 10–28. [CrossRef]
9. Kurniawan, Y.S.; Sathuluri, R.R.; Ohto, K. Droplet microfluidic device for rapid and efficient metal separation using host-guest chemistry. In *Advances in Microfluidic Technologies for Energy and Environmental Applications*; Ren, Y., Ed.; IntechOpen: London, UK, 2020; pp. 1–19. [CrossRef]
10. Islam, M.M.; Georghiou, P.E.; Rahman, S.; Yamato, T. Calix[3]arene-analogous metacyclophanes: Synthesis, structures and properties with infinite potential. *Molecules* **2020**, *25*, 4202. [CrossRef]
11. Ahmadzadeh, S.; Kassim, A.; Rezayi, M.; Rounaghi, G.H. Thermodynamic study of the complexation of *p*-isopropylcalix[6]arene with Cs^+ cation in dimethylsulfoxide-acetonitrile binary media. *Molecules* **2011**, *16*, 8130–8142. [CrossRef]
12. Bhatt, M.; Maity, D.; Hingu, V.; Suresh, E.; Ganguly, B.; Paul, P. Functionalized calix[4]arene as a colorimetric dual sensor for Cu(II) and cysteine in aqueous media: Experimental and computational study. *New J. Chem.* **2017**, *41*, 12541–12553. [CrossRef]
13. Kurniawan, Y.S.; Ryu, M.; Sathuluri, R.R.; Iwasaki, W.; Morisada, S.; Kawakita, H.; Ohto, K.; Maeki, M.; Miyazaki, M.; Jumina, J. Separation of Pb(II) ion with tetraacetic acid derivative of calix[4]arene by using droplet-based microreactor system. *Indones. J. Chem.* **2019**, *19*, 368–375. [CrossRef]
14. Zadmard, R.; Hokmabadi, F.; Jalali, M.R.; Akbarzadeh, A. Recent progress to construct calixarene-based polymers using covalent bonds: Synthesis and applications. *RSC Adv.* **2020**, *10*, 32690–32722. [CrossRef]
15. Kurniawan, Y.S.; Sathuluri, R.R.; Iwasaki, W.; Morisada, S.; Kawakita, H.; Ohto, K.; Miyazaki, M.; Jumina, J. Microfluidic reactor for Pb(II) ion extraction and removal with amide derivative of calix[4]arene supported by spectroscopic studies. *Microchem. J.* **2018**, *142*, 377–384. [CrossRef]
16. Amr, A.E.G.; Al-Omar, M.A.; Kamel, A.H.; Elsayed, E.A. Single-piece solid contact Cu^{2+}-selective electrodes based on a synthesized macrocyclic calix[4]arene derivatives as a neutral carrier ionophore. *Molecules* **2019**, *24*, 920. [CrossRef]
17. Sadamatsu, H.; Hanada, T.; Morisada, S.; Kawakita, H.; Ohto, K. Comprehensive comparison of alkali metal extraction with a series of calix[4]arene derivatives with propyl and/or acetic acid groups. *J. Incl. Phenom. Macrocycl. Chem.* **2016**, *84*, 87–97. [CrossRef]
18. Sathuluri, R.R.; Kurniawan, Y.S.; Kim, J.Y.; Maeki, M.; Iwasaki, W.; Morisada, S.; Kawakita, H.; Miyazaki, M.; Ohto, K. Droplet-based microreactor system for stepwise recovery of precious metal ions from real metal waste with calix[4]arene derivatives. *Sep. Sci. Technol.* **2018**, *53*, 1261–1272. [CrossRef]
19. Yang, L.; Zhao, Y.; Su, Y.; Chen, G. An experimental study of copper extraction characteristics in a T-junction microchannel. *Chem. Eng. Technol.* **2013**, *36*, 985–992. [CrossRef]
20. Jiang, F.; Yin, S.; Srinivaskannan, C.; Li, S.; Peng, J. Separation of lanthanum and cerium from chloride medium in presence of complexing agent along with EHEHPA (P507) in a serpentine microreactor. *Chem. Eng. J.* **2018**, *334*, 2208–2214. [CrossRef]
21. Jafari, O.; Rahimi, M.; Kakavandi, F.H. Liquid-liquid extraction in twisted micromixers. *Chem. Eng. Proc.* **2016**, *101*, 33–40. [CrossRef]
22. Guan, Q.; Urness, K.N.; Ormond, T.K.; David, D.E.; Ellison, G.B.; Daily, J.W. The properties of a microreactor for the study of the unimolecular decomposition of large molecules. *Int. Rev. Phys. Chem.* **2014**, *33*, 447–487. [CrossRef]
23. Bao, B.; Wang, Z.; Thushara, D.; Liyanage, A.; Gunawardena, S.; Yang, Z.; Zhao, S. Recent advances in microfluidics-based chromatography—A mini review. *Separations* **2021**, *8*, 3. [CrossRef]
24. Gutierrez-Serpa, A.; Pacheco-Fernandez, I.; Pasan, J.; Pino, V. Metal-organic frameworks for solid-phase microextraction devices—A review. *Separations* **2019**, *6*, 47. [CrossRef]

25. Ahmed, I.; Akram, Z.; Bule, M.H.; Iqbal, H.M.N. Advancements and potential applications of microfluidic approaches—A review. *Chemosensors* **2018**, *6*, 46. [CrossRef]
26. Hake, V.; Sonawane, S.; Anandan, S.; Sonawane, S.; Ashokkumar, M. Process intensification approach using microreactors for synthesizing nanomaterials—A critical review. *Nanomaterials* **2021**, *11*, 98. [CrossRef] [PubMed]
27. Gupta, A.; Kumar, R. Effect of geometry on droplet formation in the squeezing regime in a microfluidic T-junction. *Microfluid. Nanofluid.* **2010**, *8*, 799–812. [CrossRef]
28. Singh, K.K.; Renjith, A.U.; Shenoy, K.T. Liquid-liquid extraction in microchannels and conventional stage-wise extractors: A comparative study. *Chem. Eng. Proc.* **2015**, *98*, 95–105. [CrossRef]
29. Sahu, A.; Vir, A.B.; Molleti, L.N.S.; Ramji, S.; Pushpavanam, S. Comparison of liquid-liquid extraction in batch systems and micro-channels. *Chem. Eng. Proc.* **2016**, *104*, 190–200. [CrossRef]
30. Yao, X.; Zhang, Y.; Du, L.; Liu, J.; Yao, J. Review of the applications of microreactors. *Renew. Sustain. Energy Rev.* **2015**, *47*, 519–539. [CrossRef]
31. Ciceri, D.; Mason, L.R.; Harvie, D.J.E.; Perera, J.M.; Stevens, G.W. Modelling of interfacial mass transfer in microfluidic solvent extraction: Part II. Heterogeneous transport with chemical reaction. *Microfluid. Nanofluid.* **2013**, *14*, 213–224. [CrossRef]
32. Ciceri, D.; Peera, J.M.; Stevens, G.W. The use of microfluidic devices in solvent extraction. *J. Chem. Technol. Biotechnol.* **2013**, *89*, 771–786. [CrossRef]
33. Ghaini, A.; Kashid, M.N.; Agar, D.W. Effective interfacial area for mass transfer in the liquid-liquid slug flow capillary microreactors. *Chem. Eng. Proc.* **2010**, *49*, 356–366. [CrossRef]